NANO LETTERS

2007
Vol. 7, No. 3
657−662

Mechanically Responding Nanovalves Based on Polyelectrolyte Multilayers

Damien Mertz,[†,‡] Joseph Hemmerlé,[†,‡] Jérôme Mutterer,[§] Sophie Ollivier,[||] Jean-Claude Voegel,[†,‡] Pierre Schaaf,*[,⊥] and Philippe Lavalle[†,‡]

Institut National de la Santé et de la Recherche Médicale, INSERM Unité 595, 11 rue Humann, 67085 Strasbourg Cedex, France, Faculté de Chirurgie Dentaire, Université Louis Pasteur, 1 Place de l'Hôpital, 67000 Strasbourg, France, Institut de Biologie Moléculaire des Plantes, Centre National de la Recherche Scientifique, 12 rue du Général Zimmer, 67084 Strasbourg Cedex, France, Institut de Chimie des Surfaces et Interfaces, Centre National de la Recherche Scientifique, UPR9069, 15 rue Jean Starcky, BP2488, 68057 Mulhouse, France, and Centre National de la Recherche Scientifique, UPR22, Institut Charles Sadron, 6 rue Boussingault, 67083 Strasbourg Cedex, France

Received November 14, 2006; Revised Manuscript Received December 15, 2006

ABSTRACT

The alternate deposition of exponentially and linearly growing polyelectrolyte multilayers leads to the formation of multicompartment films. In this study, a new system consisting in nanometer-sized multilayer barriers deposited on or between multilayer compartments was designed to respond to mechanical stimuli and to act as nanovalves. The diffusion of polyelectrolytes through the barrier from one compartment to another can be switched on/off by tuning the mechanical stretching and thereby opening or closing nanopores in the barrier. This work represents a first step toward the design of chemically or biologically active films responding to mechanical stresses.

The alternate deposition of polyanions and polycations on charged surfaces leads to the formation of nanostructured films called polyelectrolyte multilayers.[1] The layer-by-layer deposition constitutes a formidable tool to functionalize surfaces and its potential applications are optical coatings,[2] filtration devices,[3] self-supported membranes with highly enhanced Young's moduli,[4,5] fuel cell membranes,[6] biologically active membranes,[7] drug release,[8−10] or biologically active coatings.[11−14] There exist two kinds of multilayers: those whose thickness and mass increase linearly with the number of deposition steps[1] and those which grow exponentially.[15−17] Linearly growing films are usually dense, nicely structured,[1] a few tens of nanometers thick, and act as impermeable barriers for the diffusion of polyelectrolytes and even of small ions.[18] On the other hand exponentially growing films are more gel-like,[19] allow for the diffusion through the film section of polyelectrolytes[20] and even proteins, and reach thicknesses up to a few micrometers within a few deposition steps. These films can be loaded with bioactive compounds[21,22] and then act as reservoirs able to deliver such molecules to surrounding cells.[23] Recently we designed multiple strata films composed of the alternation of linearly and exponentially growing films that allows construction of multicompartment architectures where the linearly growing films act as barriers.[24] The barriers prevent the diffusion of active compounds between two compartments, meaning from the upper compartment to the lower one, and inversely. These multicompartment films are anticipated to be ideal architectures to create multifunctionalized surfaces with time scheduled activity[25] or should allow design new types of coatings where reactions between chemicals present in different compartments are induced by external stimuli. This, however, requires the opening of the barriers by the stimuli.

In this article we demonstrate that some linearly growing films can act as mechanically responsive nanosized barriers. Mechanical stretching allows opening of such barriers in a reversible manner. These barriers thus act as nanovalves. To built multicompartment films, polymeric strata playing the role of reservoirs are composed of poly(L-lysine)/hyaluronic acid (PLL/HA) films. PLL/HA multilayers are known to grow exponentially and PLL chains diffuse over the entire architecture.[20] On the other hand poly(diallyldimethylam-

* Corresponding author. Telephone number: +33 (0)3 88 41 40 12. Fax number: +33 (0)3 88 41 40 99. E-mail address: schaaf@ics.u-strasbg.fr.
† Institut National de la Santé et de la Recherche Médicale, INSERM Unité 595.
‡ Faculté de Chirurgie Dentaire, Université Louis Pasteur.
§ Institut de Biologie Moléculaire des Plantes, Centre National de la Recherche Scientifique.
|| Institut de Chimie des Surfaces et Interfaces, Centre National de la Recherche Scientifique, UPR9069.
⊥ Centre National de la Recherche Scientifique, UPR22, Institut Charles Sadron.

10.1021/nl062657+ CCC: $37.00
Published on Web 02/09/2007

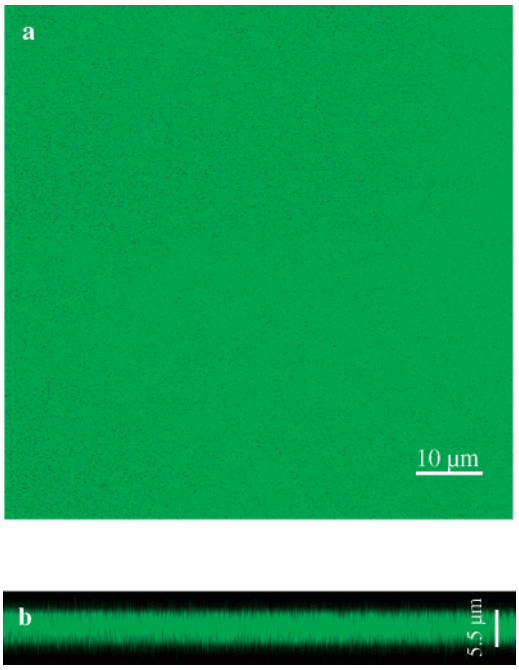

Figure 1. Confocal laser scanning microscope (CLSM) images of a $(PLL/HA)_{30}/PLL^{FITC}$ multilayer film deposited on a silicone sheet and observed at a stretching degree of $l/l_0 = 2$ (stretching degree of 1 corresponds to the initial length l_0 of the silicone sheet): (a) top view (x,y) (77×77 μm^2); (b) cross section view (x,z) (77×11 μm^2). The total thickness of the film is around 5.5 μm.

monium chloride)/poly(styrene sulfonate) (PDADMA/PSS) multilayers which are known to be linearly growing films with stratified architectures[26] will act as barrier strata when inserted between two PLL/HA compartments and thus prevent PLL chain diffusion between different compartments.

The multicompartment films are deposited on bare silicon sheets acting as elastomer substrates (see Supporting Information for experimental details). Multicompartment films are constructed by dipping the substrate alternately in the polycation and polyanion solutions. Each polyelectrolyte deposition is followed by a rinsing step by dipping the substrate in the buffer solution. Film buildup is always initiated by depositing a $(PLL/HA)_{30}$ multilayer stratum on the bare silicone sheet. On top of the $(PLL/HA)_{30}$ multilayer, green fluorescently labeled poly(L-lysine) chains (PLL^{FITC}) (FITC, fluoresceine isothiocyanate) are deposited, leading to a complete labeling of the film section as previously described.[20] The thickness of the entire film is around 5 μm. This multilayer film is then submitted to a longitudinal stretching under a confocal laser scanning microscope (CLSM). The stretch degree is defined by the parameter l/l_0 where l_0 and l correspond to the initial length and to the stretched length of the silicone sheet, respectively. Up to an elongation of 2 of the $(PLL/HA)_{30}/PLL^{FITC}$ film, no breakage or defect is visible, at least at the length scale of the CLSM (Figure 1). This demonstrates the strong adhesion of these PLL/HA multilayers on the silicone substrate and it also confirms their gel-like properties.[27]

The $(PLL/HA)_{30}/PLL$ multilayer is then capped with a $(PSS/PDADMA)_n$ multilayer. The buildup of both strata multilayer films is checked with a quartz crystal microbalance to control the regular change in frequency and dissipation corresponding to the layer-by-layer deposition process and the thickness of the $(PSS/PDADMA)_n$ bilayer is valued at 14 nm per bilayer (See Figure 1 of Supporting Information II). Such a (PSS/PDADMA) multilayer being used as a barrier for the first time, its efficiency to prevent diffusion of PLL^{FITC} chains from the solution into the reservoir is first checked with CLSM. This is performed by constructing a film with a PLL/HA compartment entirely labeled with PLL^{Rho} (red fluorescence from PLL chains labeled with rhodamine succinimidyl ester) and capped with $n = 2$, 5, 15, and 30 bilayers of PSS/PDADMA. Then, the resulting film corresponding to $(PLL/HA)_{30}/PLL^{Rho}/(HA/PLL)/(PSS/PDADMA)_n$ architecture is brought in contact with a PLL^{FITC} solution (0.5 mg·mL^{-1}). No green color is detected in the film section over more than 8 h (see as an example, Figure 2a for $n = 5$) proving that $(PSS/PDADMA)_n$ multilayers act as barriers toward PLL diffusion. We also verify that these multilayer barriers continue to prevent PLL diffusion when a $(PLL/HA)_{30}$ compartment is deposited on their top.

Next, the behavior of the $(PLL/HA)_{30}/PLL^{Rho}/HA/PLL/(PSS/PDADMA)_n$ films under stretching is investigated for various architectures ($n = 2$, 5, 15, and 30). The films in contact with PLL^{FITC} solutions are observed with CLSM. By gradually increasing the stretching, a critical stretching degree is reached where the $(PSS/PDADMA)_n$ films become inefficient to play the barrier role for preventing PLL chain diffusion from the solution to the underlying PLL/HA compartment. This critical stretching degree depends on the number n of bilayers constituting the barrier and increases with n. The results are summarized in Table 1. For stretching degrees higher than the critical stretching degree, PLL^{FITC} chains from the solution diffuse into the $(PLL/HA)_{30}$ compartment as can be seen in Figure 2b for $n = 5$ and for a stretching degree of $l/l_0 = 1.5$. Once the barrier opens up for stretching degrees exceeding the critical value, PLL chains diffuse within a few minutes inside the $(PLL/HA)_{30}$ film. The final PLL^{FITC} concentration in the film by far exceeds the PLL^{FITC} concentration in the solution. Figure 3a illustrates the CLSM observation of the $(PLL/HA)_{30}/PLL^{Rho}/HA/PLL/(PSS/PDADMA)_5$ film incubated in a PLL^{FITC} solution when no stretching is applied. The two-dimensional view (x,y) at the film/solution interface depicts a homogeneous film at the scale of the CLSM resolution without any defects in the structure. For stretching degrees smaller than $l/l_0 = 1.4$ interfaces show similar features with high homogeneity. When silicone sheets are stretched at $l/l_0 = 1.5$, which is above the critical stretching degree for $n = 5$, small black spots corresponding to nonlabeled pores appear on top of the film (Figure 3b). Their size is estimated to be of the order of a few hundreds of nanometers (from 100 nm to 1 μm). These pores are only visualized when one focuses at the upper part of the film which corresponds to the PSS/PDADMA strata. CLSM imaging of (x,y) planes inside the films shows uniform green fluorescence indicating that the pores are only located in the $(PSS/PDADMA)_n$ barrier and do not extend down to the PLL/HA compartment. The

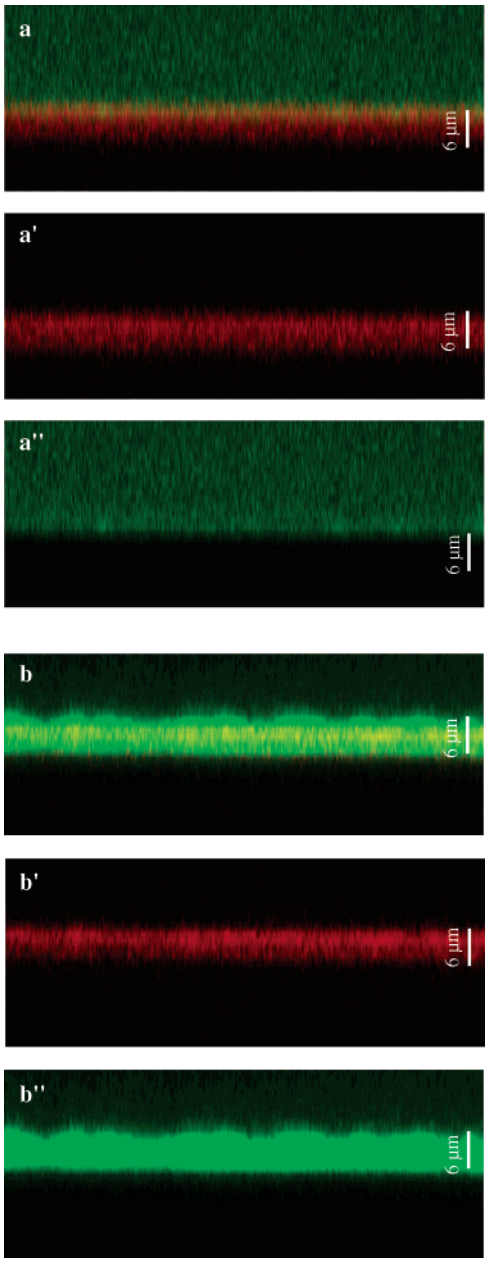

Figure 2. CLSM section images (x,z views) of a $(PLL/HA)_{30}/PLL^{Rho}/(HA/PLL)/(PSS/PDADMA)_5$ multilayer film (one compartment capped with a barrier) deposited on a silicone sheet and brought in contact with a PLL^{FITC} solution. Observations are performed before stretching (a, a′, and a″) and at a stretching degree of $l/l_0 = 1.5$ (b, b′, and b″). Film sections are observed (a, b) in the red and green channels, (a′ and b′) in the red channel only, and (a″ and b″) in the green channel only. The total thickness of the multilayer film labeled in red is around 6 μm. Image sizes are 77 $\times$ 30 μm^2.

appearance of pores under stretching is also confirmed by atomic force microscopy (AFM) on a similar sample for a stretching degree of $l/l_0 = 2$ (Figure 4). The characteristic sizes of the holes are of the order of 150−1500 nm in accordance with the CLSM measurements. For barriers constituted of less ($n = 2$) or more ($n = 15$ and 30) than $n = 5$ PSS/PDADMA strata, the same conclusions can be drawn: below the critical stretching degree, the films remain homogeneous and for stretching degrees higher than this

Table 1. Critical Stretching Degrees of the Silicone Sheet as a Function of the Number of Bilayers, n, Constituting the PSS/PDADMA Barrier[a]

n	critical stretching degrees	n	critical stretching degrees
2	1.1	15	1.9−2.0
5	1.3−1.4	30	>2.2

[a] Below these values, the barriers ensure impermeability against PLL chains, when for higher values the barriers become inefficient to prevent PLL diffusion.

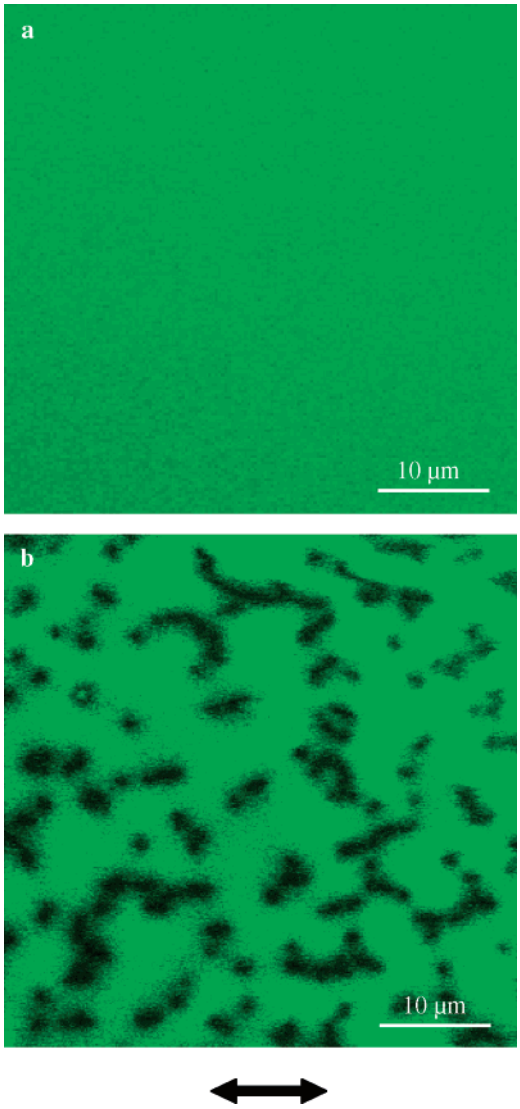

Figure 3. CLSM top view (x,y) images in the green channel of a $(PLL/HA)_{30}/PLL^{Rho}/(HA/PLL)/(PSS/PDADMA)_5$ multilayer film (one compartment capped with a barrier) deposited on a silicone sheet and brought in contact with a PLL^{FITC} solution: (a) The silicone sheet is not stretched. (b) The silicone sheet with the multilayers is stretched at $l/l_0 = 1.5$. The black arrow indicates the stretching direction. Image sizes are 47 $\times$ 47 μm^2.

critical value, pores appear in the barrier layer. The permeability of the barriers against PLL chains is related to the presence of these nanopores and can thus be finely controlled by the stretching degree applied on the film.

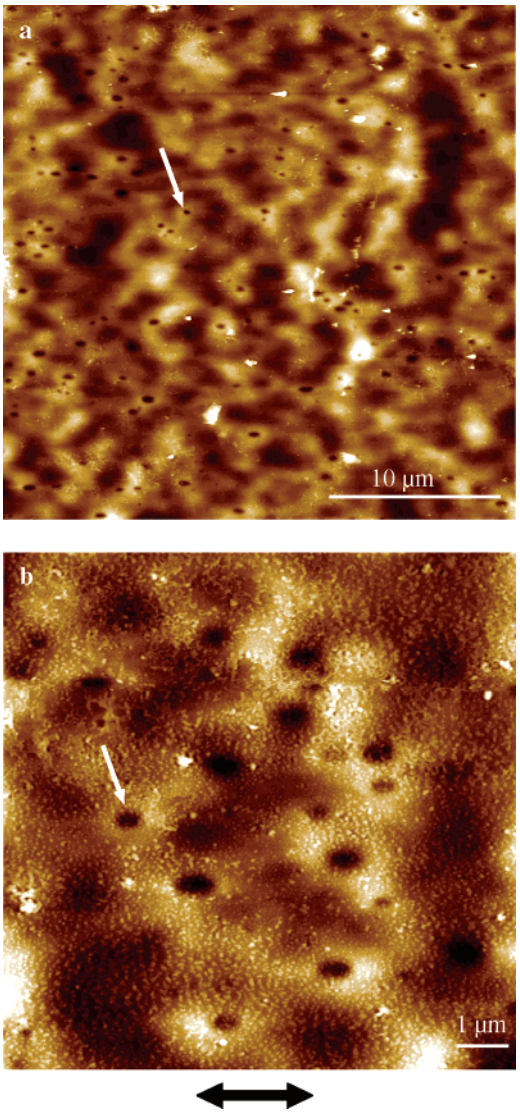

Figure 4. AFM images of a $(PLL/HA)_{30}/PLL/(HA/PLL)/(PSS/PDADMA)_5$ multilayer film (one compartment capped with a barrier) deposited on a silicone sheet. The silicone sheet with the multilayers is stretched at $l/l_0 = 2.0$. White arrows indicate pores in the film. The black arrow indicates the stretch direction. Image sizes are $30 \times 30\ \mu m^2$ (a) and $10 \times 10\ \mu m^2$ (b).

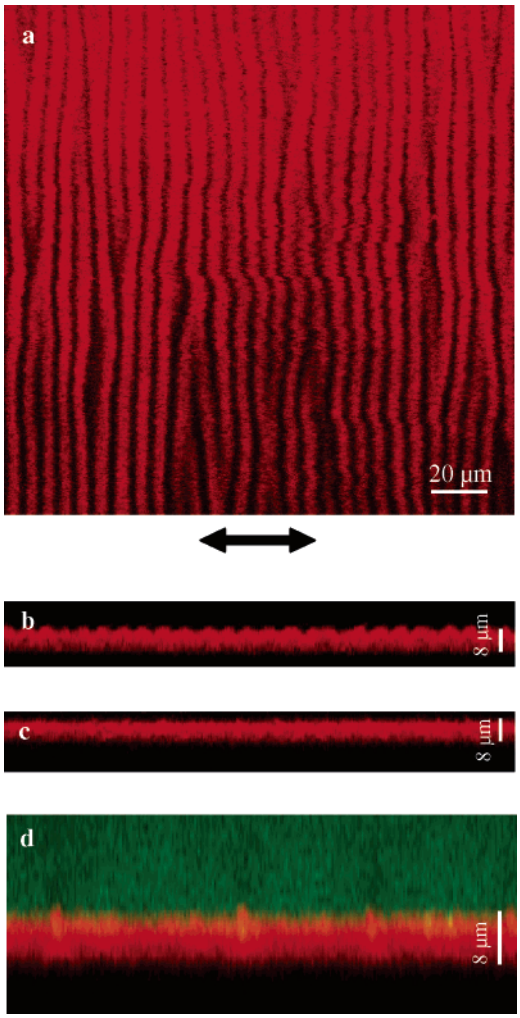

Figure 5. CLSM images of a $(PLL/HA)_{30}/PLL^{Rho}/(HA/PLL)/(PSS/PDADMA)_5$ multilayer film (one compartment capped with a barrier) deposited on a silicone sheet and observed in a nonstretched state after a stretching to a degree of $l/l_0 = 1.8$ for 30 min: (a) top view (x,y) $(182 \times 182\ \mu m^2)$ 5 min after being brought back to the nonstretched state; (b) cross section view (x,z) $(177 \times 21\ \mu m^2)$, 5 min after being brought back to the nonstretched state; (c) cross section view (x,z) $(177 \times 21\ \mu m^2)$, 30 min after being brought back to the nonstretched state; (d) cross section view (x,z) $(77 \times 30\ \mu m^2)$, the film in the nonstretched state is maintained in contact with a PLL^{FITC} solution over 1 h.

In order to investigate the reversibility of the barrier opening, a $(PLL/HA)_{30}/PLL^{Rho}/HA/PLL/(PSS/PDADMA)_5$ film is stretched 30 min up to $l/l_0 = 1.8$, corresponding to a value higher than the critical stretching degree, and then brought back to its original nonstretched state. As soon as the film is brought back to its nonstretched state, wrinkles with a periodicity about 5 μm and perpendicular to the stretching direction (y direction) appeared (Figure 5a,b). These regular structures observed on top of the red-labeled zone probably concern the reservoir/barrier interface. After the film was maintained for 30 min in a nonstretched state, wrinkles totally disappeared and the film recovers a flat and homogeneous configuration (Figure 5c). When this film is brought in contact with a PLL^{FITC} solution, no diffusion of PLL^{FITC} into the film is detected over 1 h (Figure 5d), indicating that the $(PSS/PDADMA)_5$ stratum plays again the role of a PLL-tight barrier. *These observations strongly suggest that the barrier opening and pore formation are fully reversible.* These experiments also demonstrate that both the $(HA/PLL)_{30}$ and the $(PSS/PDADMA)_5$ multilayers behave as viscous fluid-like materials leading to healing processes of the barrier.

Let us now focus on the behavior of a film composed of two compartments separated by one barrier. PLL from both $(PLL/HA)_{30}$ compartments are labeled, one with rhodamine, the other with fluorescein, leading to the following architecture: $(PLL/HA)_{30}/PLL^{Rho}/HA/PLL/(PSS/PDADMA)_5/(HA/PLL)_{30}/HA/PLL^{FITC}$. When this film is stretched below $l/l_0 = 1.4$, no diffusion of PLL from one compartment to the other is observed during the whole observation period (4 h) and both compartments materialized by green and red areas are clearly separated. The same conclusions can be drawn from observations 1 min after applying a stretching

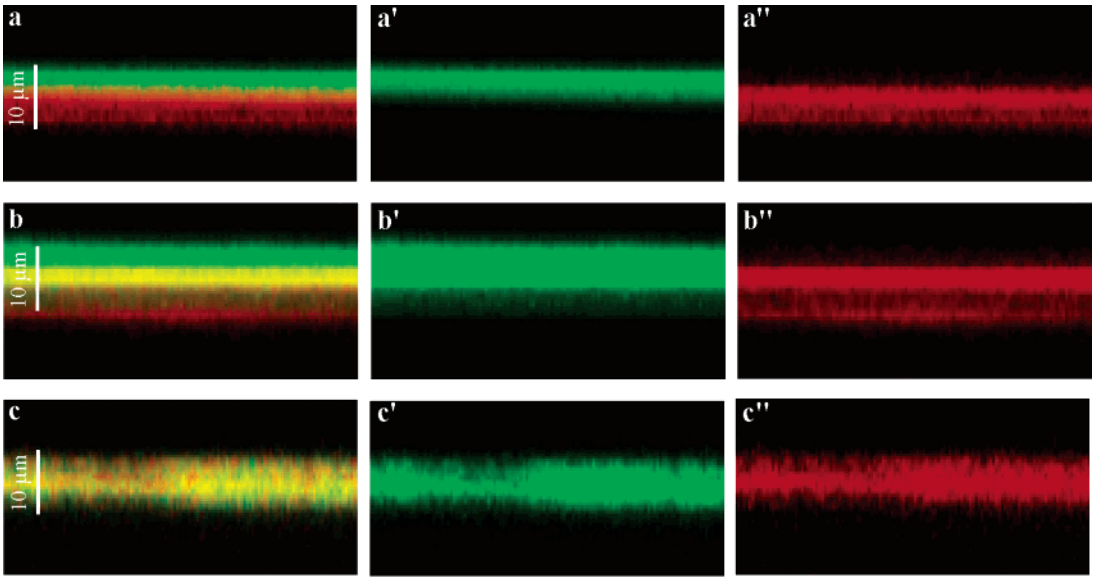

Figure 6. CLSM section images (x,z views) of a $(PLL/HA)_{30}/PLL^{Rho}/(HA/PLL)/(PSS/PDADMA)_5/(HA/PLL)_{30}/HA/PLL^{FITC}$ multilayer film (two compartments separated by a barrier) deposited on a silicone sheet maintained in a 0.15 M NaCl solution. Observations are performed after a stretching degree of 1.9 during (a) 1 min, (b) 240 min, and (c) 480 min. Panels a, b, and c correspond to x,z sections in the green and red channels, panels a′, b′, and c′ to the green channel, and panels a″, b″, and c″ to the red channel. The total thickness of the multilayer film is around 10 μm. Image sizes are 55 × 28 μm^2.

of $l/l_0 = 1.9$, a value higher than the critical stretching degree (Figure 6a). On the other hand, when the film is stretched up to $l/l_0 = 1.9$ for 4 h, a gradual diffusion of PLL^{FITC} chains from the upper to the lower compartment and a gradual diffusion of PLL^{Rho} chains from the lower to the upper compartment occurs (Figure 6b). The $(PSS/PDADMA)_5$ barrier located in the middle of the film section becomes then strongly labeled with PLL^{FITC} and PLL^{Rho}. The time scale of the diffusion of PLL chains from one compartment to the other lies in the order of 8 h (Figure 6c). After this time delay, the fluorescence through the film section is homogeneous and the two compartments can no longer be differentiated. Moreover, as for the $(PLL/HA)_{30}/PLL^{Rho}/(HA/PLL)/(PSS/PDADMA)_5$ film, the appearance of pores in the barrier separating the two compartments, under stretching degrees exceeding the critical value ($l/l_0 = 1.9$), is observed (Figure 7). Size and distribution of the pores in the film are very comparable to previous AFM observations on the multilayer capped by a barrier. Thus the upper $(PLL/HA)_n$ compartment exhibits only a minor influence on the behavior of the barrier under stretching. Once the film is brought back to its nonstretched state, wrinkles perpendicular to the stretching direction (y direction) also appeared as it is the case for the compartment/barrier system. These wrinkles also disappear after a few tens of minutes.

Our experiments do not allow access to the mechanism that leads to the formation of pores, at a molecular level. One can thus only speculate about such a mechanism. Nevertheless, preliminary experiments performed on $(PLL/HA)_{30}/PLL/(PSS/PAH)_n$ where PAH stands for poly(allyl amine hydrochloride) reveal that the $(PSS/PAH)_n$ cap also acts as a barrier but that, even under a moderate stretching degree of 1.10, cracks appear in the film (see Figure 2 of Supporting Information II). These cracks are very different

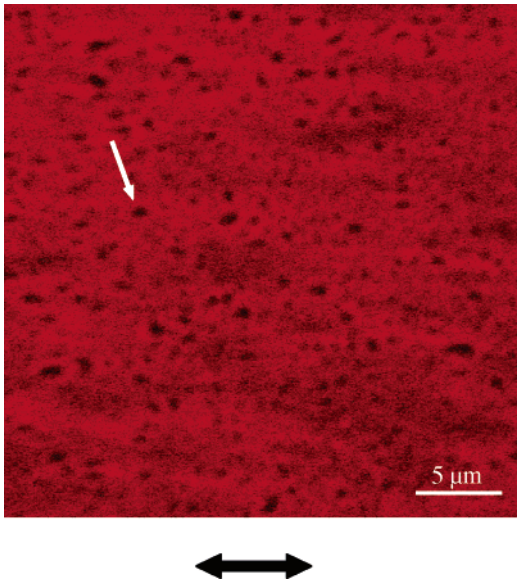

Figure 7. CLSM (x,y) image in the red channel of a $(PLL/HA)_{30}/PLL^{Rho}/(HA/PLL)/(PSS/PDADMA)_5/(HA/PLL)_{30}/HA/PLL^{FITC}$ multilayer film (two compartments separated by a barrier) focused on the $(PSS/PDADMA)_5$ barrier. The silicone sheet with the multilayers is stretched at a degree of 1.9. White arrow on the image shows an example of a pore localized in the barrier. The black arrow indicates stretching direction. Image size is 30 × 30 μm^2.

from the holes observed in the $(PSS/PDADMA)_n$ barriers. It appears as if the $(PSS/PAH)_m$ multilayers behave as a solid, brittle material, confirming the glassy nature of these films. In contrast, the $(PSS/PDADMA)_n$ films appear softer and viscoelastic. The origin of the holes seems thus not to originate from microcracking or crazing of the barrier but rather to debonding of the chains. One can assume that before stretching the thickness of the $(PSS/PDADMA)_n$ barrier is not rigorously constant over the whole film but that there

exist thickness fluctuations. Under stress due to stretching, the $(PSS/PDADMA)_n$ film reorganizes with chains that diffuse one with respect to others. The locations of smaller thickness are then the ones where the lateral stress on the chains is highest. This induces lateral diffusion of the chains and leads to a thinning of the film before the appearance of small holes. This process is entirely driven by diffusion of the chains under stress. Once the stress is removed, the diffusion of the chains leads again to an interdiffusion and interdigitation of the different polyelectrolytes of the barrier. This then constitutes the healing process.

To summarize, by alternating exponentially and linearly growing multilayers on silicone sheets, we designed multicompartment films with nanosized barriers. These barriers can be opened and reversibly closed by mechanical stretching and thus act as nanovalves. For the investigated system, the stretching induces the formation of pores in the barriers once a critical stretching degree is reached and consequently allows a diffusion process through the barrier of polyelectrolyte chains initially contained in the different compartments. This critical stretching degree depends upon the number of bilayers constituting the barrier. These architectures should allow creating films able to respond, chemically or biologically, to mechanical stimuli. In particular, the design of multicompartment films containing several barriers whose critical stretching rates decrease gradually from the substrate toward the outer part of the architecture can be considered, leading to cascades of reactions controlled by adjusting the mechanical stretching rates.

Acknowledgment. This work was supported by the ACI "Nanosciences 2004" from the Ministère de la Recherche et des Nouvelles Technologies (Project NR204). Ph. Lavalle is indebted to the Hôpitaux Universitaires de Strasbourg for financial support. We thank Jérôme Mutterer (Institut de Biologie Moléculaire des Plantes, CNRS/ULP, Strasbourg, France) for his help in performing CLSM. The CLSM platform used in this study was cofinanced by the Région Alsace, the Université Louis Pasteur, and the Association pour la Recherche sur le Cancer. We thank B. Senger for his analysis of the quartz crystal microbalance experiments. We also thank Karim Benmlih for the realization of the stretching devices. J. C. Voegel and P. Schaaf also thank Professor M. W. Hosseini for fruitful discussions.

Supporting Information Available: Detailed experimental procedures and figures showing QCM measurements monitoring changes in frequency shift, dissipation shifts, and evolution of the film thickness and confocal laser scanning microscopy view of a multilayer film. This material is available free of charge via the Internet at http://pubs.acs.org.

References

(1) Decher, G. *Science* **1997**, *277*, 1232−1237.
(2) Hiller, J.; Mendelsohn, J. D.; Rubner, M. F. *Nat. Mater.* **2002**, *1*, 59−63.
(3) Liu, X. Y.; Bruening, M. L. *Chem. Mat.* **2004**, *16*, 351−357.
(4) Mamedov, A.; Kotov, N. A.; Prato, M.; Guldi, D. M.; Wicksted, J. P.; Hirsch, A. *Nat. Mater.* **2002**, *1*, 190−194.
(5) Tang, A.; Kotov, N. A.; Magonov, S.; Ozturk, B. *Nat. Mater.* **2003**, *2*, 413−418.
(6) Farhat, T.; Hammond, P. T. *Adv. Funct. Mater.* **2005**, *15*, 945−954.
(7) Onda, M.; Lvov, Y.; Ariga, K.; Kunitake, T. *J. Ferment. Bioeng.* **1996**, *82*, 502−506.
(8) Berg, M. C.; Zhai, L.; Cohen, R. E.; Rubner, M. F. *Biomacromolecules* **2006**, *7*, 357−364.
(9) Izumrudov, V. A.; Kharlampieva, E.; Sukhishvili, S. A. *Biomacromolecules* **2005**, *6*, 1782−1788.
(10) Vazquez, E.; Dewitt, D. M.; Hammond, P. T.; Lynn, D. M. *J. Am. Chem. Soc.* **2002**, *124*, 13992−13993.
(11) Benkirane-Jessel, N.; Lavalle, P.; Hübsch, E.; Holl, V.; Senger, B.; Haïkel, Y.; Voegel, J.-C.; Ogier, J.; Schaaf, P. *Adv. Funct. Mater.* **2005**, *15*, 648−654.
(12) Thierry, B.; Kujawa, P.; Tkaczyk, C.; Winnik, F. M.; Bilodeau, L.; Tabrizian, M. *J. Am. Chem. Soc.* **2005**, *127*, 1626−1627.
(13) Jessel, N.; Oulad-Abdelghani, M.; Meyer, F.; Lavalle, P.; Haikel, Y.; Schaaf, P.; Voegel, J. C. *Proc. Natl. Acad. Sci. U.S.A.* **2006**, *103*, 8618−8621.
(14) Cortez, C.; Tomaskovic-Crook, E.; Johnston, A. P. R.; Radt, B.; Cody, S. H.; Scott, A. M.; Nice, E. C.; Heath, J. K.; Caruso, F. *Adv. Mater.* **2006**, *18*, 1998−2003.
(15) Elbert, D. L.; Herbert, C. B.; Hubbell, J. A. *Langmuir* **1999**, *15*, 5355−5362.
(16) Picart, C.; Lavalle, P.; Hubert, P.; Cuisinier, F. J. G.; Decher, G.; Schaaf, P.; Voegel, J.-C. *Langmuir* **2001**, *17*, 7414−7424.
(17) Kujawa, P.; Moraille, P.; Sanchez, J.; Badia, A.; Winnik, F. M. *J. Am. Chem. Soc.* **2005**, *127*, 9224−9234.
(18) Farhat, T.; Schlenoff, J. B. *Langmuir* **2001**, *17*, 1184−1192.
(19) Kulcsar, A.; Lavalle, P.; Voegel, J. C.; Schaaf, P.; Kékicheff, P. *Langmuir* **2004**, *20*, 282−286.
(20) Picart, C.; Mutterer, J.; Richert, L.; Luo, Y.; Prestwich, G. D.; Schaaf, P.; Voegel, J.-C.; Lavalle, P. *Proc. Natl. Acad. Sci. U.S.A.* **2002**, *99*, 12531−12535.
(21) Caruso, F.; Niikura, K.; Furlong, D. N.; Okahata, Y. *Langmuir* **1997**, *13*, 3427−3433.
(22) Vodouhe, C.; Le Guen, E.; Mendez Garza, J.; Francius, G.; Déjugnat, C.; Ogier, G.; Schaaf, P.; Voegel, J.-C.; Lavalle, P. *Biomaterials* **2006**, *27*, 4149−4156.
(23) Benkirane-Jessel, N.; Schwinté, P.; Falvey, P.; Darcy, R.; Haïkel, Y.; Schaaf, P.; Voegel, J.-C.; Ogier, J. *Adv. Funct. Mater.* **2004**, *14*, 174−182.
(24) Garza, J. M.; Schaaf, P.; Muller, S.; Ball, V.; Stoltz, J. F.; Voegel, J.-C.; Lavalle, P. *Langmuir* **2004**, *20*, 7298−7302.
(25) Wood, K. C.; Chuang, H. F.; Batten, R. D.; Lynn, D. M.; Hammond, P. T. *Proc. Natl. Acad. Sci. U.S.A.* **2006**, *103*, 10207−10212.
(26) Jomaa, H. W.; Schlenoff, J. B. *Macromolecules* **2005**, *38*, 8473−8480.
(27) Collin, D.; Lavalle, P.; Garza, J. M.; Voegel, J.-C.; Schaaf, P.; Martinoty, P. *Macromolecules* **2004**, *37*, 10195−10198.

NL062657+